Design and construction of GRS integral bridges for railways in Japan

Masayuki Koda, Hidetoshi Nishioka & Kenichi Kojima
Railway Technical Research Institute(RTRI), Japan

Shinichi Tamai
Japan Railway Construction Transport and Technology Agency (JRTT), Japan

Fumio Tatsuoka
Tokyo University of Science, Japan

ABSTRACT: Geosynthetic-Reinforced Soil (GRS) integral bridge was developed and constructed for the first time in Japan. A pair of GRS retaining walls (RWs) are first constructed as the main component of a pair of abutments. After the deformation of supporting ground and backfill has taken place sufficiently, a RC full-height rigid (FHR) facing is constructed by casting-in-place concrete directly on the wall face wrapped-around with geogrid layers reinforcing the backfill in such that the facing is firmly integrated to the reinforced backfill. Finally, a girder is constructed with both ends structurally integrated to the top ends of the FHR facings. Due to very-high cost effectiveness with excellent performance against not only severe seismic loads but also long-term train loads requiring minimized maintenance work, this technology has been well accepted by railway engineers in Japan. Potential problems due to annual thermal deformation and long-term concrete dry shrinkage of the girder and severe seismic loads become more serious as the span becomes longer. Several measures were developed to alleviate these problems by performing a series of cyclic loading tests on a full-scale partial model comprising a FHR facing, a buffer zone and part of approach block. The relevance of the structural design and construction method was confirmed by monitoring long-term performance of a GRS integral bridge with a span of 60 m.

Keywords: geosynthetic-reinforced soil integral bridge, long-term behavior, railway, seismic behavior

1 INTRODUCTION

A typical conventional bridge has a girder that is simple-supported by a pair of abutments via a pair of bearings (i.e., a fixed pin and a movable roller), while unreinforced approach fills are constructed retained by the abutments that have been constructed in advance. For these features of structure and construction, the following several problems are often encountered. Firstly, as the abutments are a cantilever structure, with an increase in the abutment height, the structure becomes more massive and, with a decrease in the bearing capacity of the supporting ground, needs for the use of costly piles increase to keep small the displacements of the abutments caused by earth pressure and ground movements associated with the construction of approach fills. Secondly, 1) installation of bearings with arrangements to prevent the dislodging of the girder by seismic loads; and 2) long-term maintenance preventing the corrosion of the bearings are both rather costly. Thirdly, the seismic stability of the cantilever-type abutments and unreinforced backfill is basically rather low. Fourthly, a relatively large bumping may develop immediately back of the abutment gradually by self-weight and long-term traffic loads and suddenly by seismic loads, which may be enhanced by displacements of the abutment and deformation of the supporting ground.

To alleviate these problems due to the use of bearings, integral bridges were developed and many have been constructed in the UK and the North America. This bridge type comprises a continuous girder structurally integrated to a pair of RC abutments without using bearings. However, as approach fills are unreinforced and they are constructed after the construction of the abutments, many problems with the conventional bridge type remain unsolved. Besides, a new problem develops: i.e., the backfill is cyclically displaced laterally by annual thermal deformation of the girder, which results in both residual settlement of the backfill by active failure and development of high passive earth pressure (i.e., a dual ratcheting phenomenon; Tatsuoka et al., 2009, 2010, 2018). Results from a series of model tests showed that these

problems can be effectively alleviated while maintaining the advantages of integral bridge by reinforcing the backfill with reinforcement layers connected to the back of the full-height rigid (FHR) facings. This new type bridge is called Geosynthetic-Reinforced Soil (GRS) integral bridge (Fig. 1). Following the construction method of GRS RW with FHR facing (Tatsuoka et al., 1997), after the deformation of the supporting ground and the backfill associated with the construction of the reinforced backfill has taken place sufficiently, lightly steel-reinforced FHR facings are constructed by casting-in-place concrete on the wall face wrapped-abound with geogrid layers reinforcing the backfill. By this staged-construction and as the FHR facing becomes a continuous beam supported by reinforcement layers at many elevations (Tatsuoka 1992), the internal forces and the lateral thrust forces and overturning moment at the facing base become very small compared with the abutments of the conventional type bridge. For this reason, pile foundations becomes unnecessary in usual cases. Due to structural integration among the girder, the FHR facings and the reinforced backfill, the forces activated in the girder and facings become much lower than those in the simple-supported girder. As a result, the girder and facings (i.e., abutments) of GRS integral bridge are much less massive than those of the conventional type bridge under otherwise the same conditions.

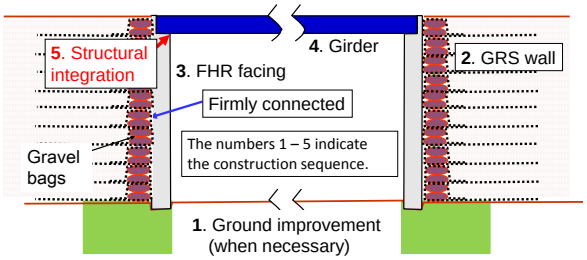

Figure 1. Structure of GRS integral bridge: the numbers denote the construction sequence.

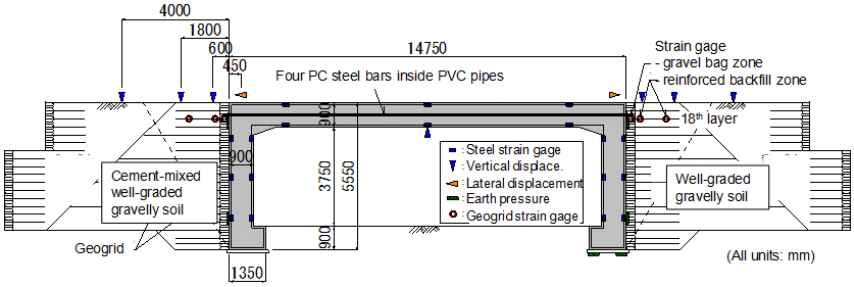

Figure 2. Full-scale model of GRS integral bridge (Nagatani et al., 2009; Koda et al. 2013).

Figure 3. A general view of the model with arrangements for lateral cyclic loading tests (Koda et al., 2013).

To establish the construction and design procedures of this new type bridge, a full-scale model of GRS integral bridge comprising a 14.75 m-long and 3 m-wide girder integrated to a pair of 5.55 m-high abutments with backfill of either cement-mixed gravelly soil or uncemented gravelly soil was constructed at Railway Technical Research Institute by the beginning of 2009 (Fig. 2). Careful observation for two years showed that post-construction residual deformation of the RC members and the approach blocks were very small. To validate high performance of GRS integral bridge also against thermal effects and severe seismic loads, a series of lateral cyclic loading tests were performed in the bridge axis direction of the model in Feb. 2011 (Fig. 3; Koda et al., 2013). In cyclic loading tests simulating thermal effects of a temperature change of 20^{o} in centigrade, no significant increase took place in the earth pressure on the back of the facing with negligible settlement at the backfill crest. In reversed lateral cyclic loading tests simulating seismic loads, the lateral load equivalent to the inertia of the girder by L2 design seismic load (i.e., the highest seismic load likely to take place in the future during a given life time) was fully applied to the girder. Despite some noticeable effects: i.e., the tensile forces in the geogrid reaching its rupture strength at some places; thin tensile cracks on the crest of the approach blocks: and a horizontal tensile crack at the

construction joint of the FHR facing, the damage level was substantially below the level requiring repair works, showing a very high seismic stability of GRS integral bridge.

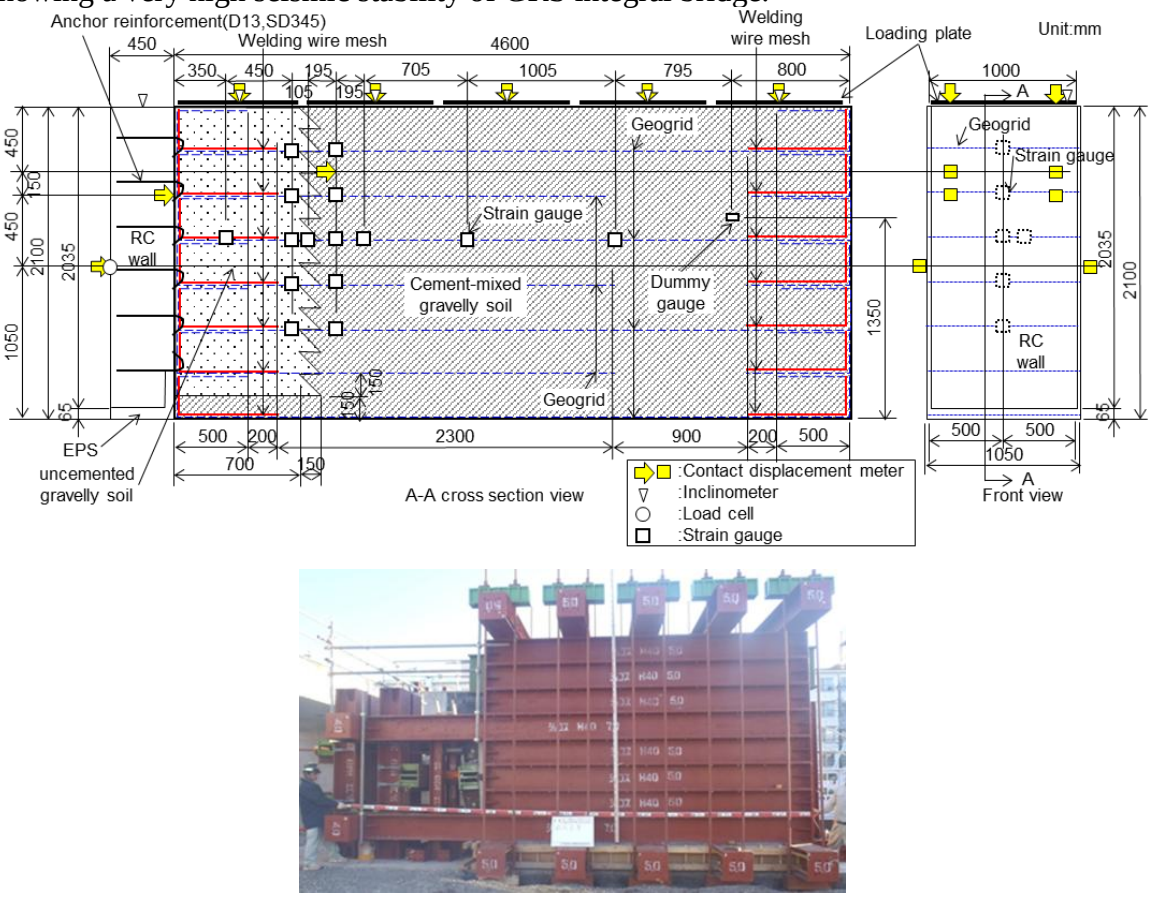

Figure 4. Full-scale partial model consisting of a FHR facing, a buffer zone and part of approach block of GRS integral bridge arranged in a loading frame.

With GRS integral bridges, effects of annual thermal deformation and long-term concrete dry shrinkage of the girder and seismic loads on the residual stresses in the girder become more serious as the span increases. As the span becomes longer than about 20 m, a specific design of the buffer zone between the facing and the approach block of cement-mixed gravelly soil becomes necessary and its properties should be carefully evaluated to be taken into account in the design. In view of the above, a series of cyclic loading tests were performed on a full-scale partial model of the abutment consisting of a FHR facing, a buffer zone and part of the approach block. Figure 4 shows this full-scale model arranged in a loading frame. To confirm the relevance of the structural design adopted based on results of these model tests, the performance of a prototype GRS integral bridge with a 60 m-long span (shown in Fig. 9) was observed from during construction and for several years after completion. This paper summarizes these experiences.

2 CYCLIC LOADING TESTS OF FULL-SCALE PARTIAL MODEL OF GRS INTEGRAL BRIDGE

The model (Fig. 4), 1.0 m-wide, 2.1 m-high and 5.05 m-long under plane strain conditions, was constructed in a steel soil container assembled with reaction frames for static vertical loading and cyclic lateral loading. To minimize wall friction, composite panels smeared with a grease layer were arranged on the inner faces of the soil container. The approach block consisted of 30 cm-thick layers of gravelly soil (M40) mixed with cement 3% in dry weight of gravel sandwiched with geogrid layers arranged in a vertical spacing of 30 cm. Each 30 cm-thick soil layer consisted of four 7.5 cm-thick sub-layers compacted to 95.5 % of the maximum dry density by Modified Proctor. Unconfined compression tests were performed on specimens (20 cm in diameter & 40 cm in height) of the cemented gravelly soil cured for a period of 56 days as in the full-scale model loading. The average unconfined compression strength was 7.1 MPa. The design tensile rupture strength (T_k) of the geogrid was 101 kN/m, while the length was 4.6 m with longer ones and 3.0 m with shorter ones (Fig. 4). Fig. 5 shows the structure of the buffer zone. A welding wire mesh framework (Fig. 5c) was used to form a temporary facing until the construction of a 2.1 m-high RC FHR facing by casting-in-place fresh concrete directly on the welding wire mesh wrapped

around with a geogrid sheet (Fig. 5b). The total ultimate tensile rupture strength for all the six geogrid layers was estimated to be about 650 kN, while the total connection strength between the FHR facing and the welding wire meshes was estimated to be about 250 kN with a 95% confidence based on the previous experiment. As the total strength of these two components may not be sufficient when subjected to severe seismic loads simulated in the tests, six layers of four steel rods (D13, L=350 mm) were anchored in welding wire meshes (Figs. 5a & 5b). Compacted unbound gravelly soil filled each 70 cm-long welding wire mesh framework and a 30 cm-long free zone between the tail end of the welding wire mesh and the front face of the approach block arranged to effectively absorb cyclic lateral deformation due to thermal changes in the girder length and seismic loading.

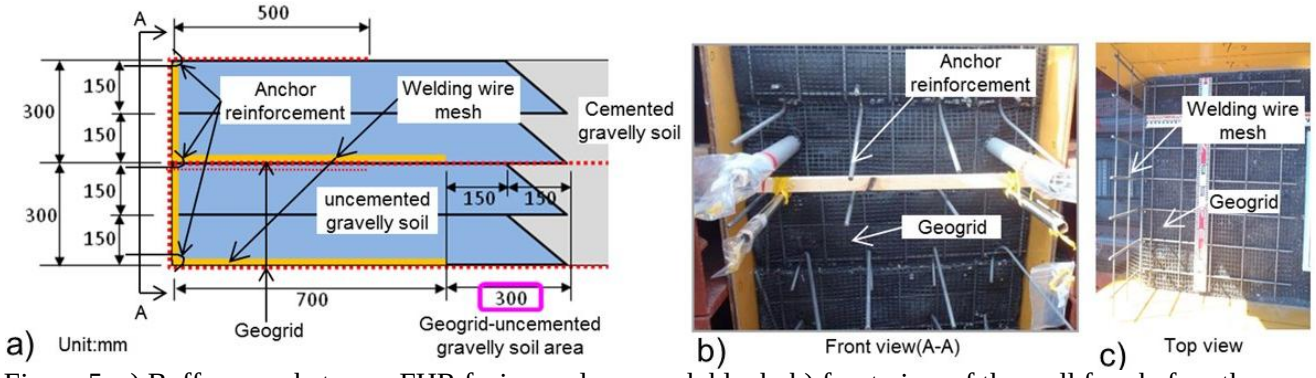

Figure 5. a) Buffer zone between FHR facing and approach block; b) front view of the wall face before the construction of FHR facing; and c) top view of the welding wire mesh before placing gravelly soil.

A total vertical load of 500 kN (i.e., an average vertical pressure of 109 kPa) was applied to the crest of the buffer zone and the approach block by means of a set of center-hole hydraulic jacks arranged at the top of the vertical PC steel rods that connected five top 5 m-long steel reaction beams to five bottom 7 m-long steel reaction beams (Fig. 4). 500 kN was a sum of 161 kN (an assumed weight of road bed and train load) and 339 kN (the weight of overlying 3.2 m-high backfill). Lateral load was applied to the top 1.8 m-thick zone, underlain by an unloaded 0.3 m-thick bottom zone, of the 2.1 m-thick model. This load simulated the load applied to the bottom 1.8 m-thick zone of a 5.0 m-high wall. A vertical load of 500 kN was necessary to apply large lateral loads to the model without slipping at the model base. Tensile lateral load in the active direction was applied by means of a pair of center-hole hydraulic jacks arranged at the end of horizontal PC rods connected to 1/4 and 3/4 heights of the FHR facing. Compressive lateral load in the passive direction was applied to the central height of the FHR facing by means of a hydraulic jack. As listed in Table 1, Cases 1, 2 and 3 simulated lateral loading by thermal deformation and concrete drying shrinkage of the girder. The number of loading cycles was 5 in Case 1 and 15 in Cases 2 and 3. Case 4 simulated seismic loading. The methods to measure several physical quantities are indicated in Fig. 4.

Table 1. Cyclic loading tests.

Test case	Simulated loading factors	Assumed girder span (m)	Maximum displacement (mm)	
			Tensile loading	Compressive loading
Case 1	Thermal deformation and drying shrinkage of concrete**	20	4	-1
Case 2		40	8	-2
Case 3		60	12	-3
Case 4	Seismic loading	-	5, 10, 15, 20, 30, 40 & 70	Load control*

*: Compressive load of the same magnitude as the tensile load was applied at each stage.
**: Assumed thermal change= ± 25°; and assumed drying shrinkage of concrete= 150 μ.

Fig. 6 shows the relationships between the lateral load (positive in tension) and the lateral displacement at the facing (positive in the active mode) in Cases 1 through 4. The largest peak tensile load in Cases 1, 2 and 3 (simulating effects of thermal deformation and drying shrinkage of concrete) was about 270 kN, which is much lower than the nominal tensile rupture strength when all the geogrid strands are equally strained, equal to 624.3 kN/m = 2.4 kN/per strand (i.e., tensile load at a design rupture strain equal to 5 %) times the total number of geogrid strand. Besides, all the cyclic relations are stable not exhibiting any sudden post-peak degradation. These results suggest insignificant damage to the geogrid in the buffer zone, if any, in Cases 1, 2 and 3. However, in each case, with cyclic loading to the same peak lateral displacement, the peak tensile load gradually decreases with a gradual decrease in the average stiffness. This is due likely to a gradual decrease in the restraint of welding wire mesh and unbound gravelly soil on the

tensile deformation of the geogrid in the buffer zone. In Case 4 (simulating severe seismic loading), when the displacement became about 25 mm, a peak tensile load equal to about 350 kN was exhibited followed by obvious post-peak degradation. 350 kN is only about a half of the nominal total tensile rupture strength (624.3 kN). It is likely that the geogrid strands were not uniformly strained, but the tensile rupture of the geogrid layers took place progressively although it was attempted to apply uniform strain. At subsequent loading stages, the peak tensile load decreased with an increase in the active facing displacement, during which tensile rupture of some geogrid layers were noticed by rupture sound. Yet, the geogrid layers in the buffer zone did not exhibit brittle tensile failure, maintaining a rather constant residual resistance of about 200 kN at least until the displacement became about 70 mm.

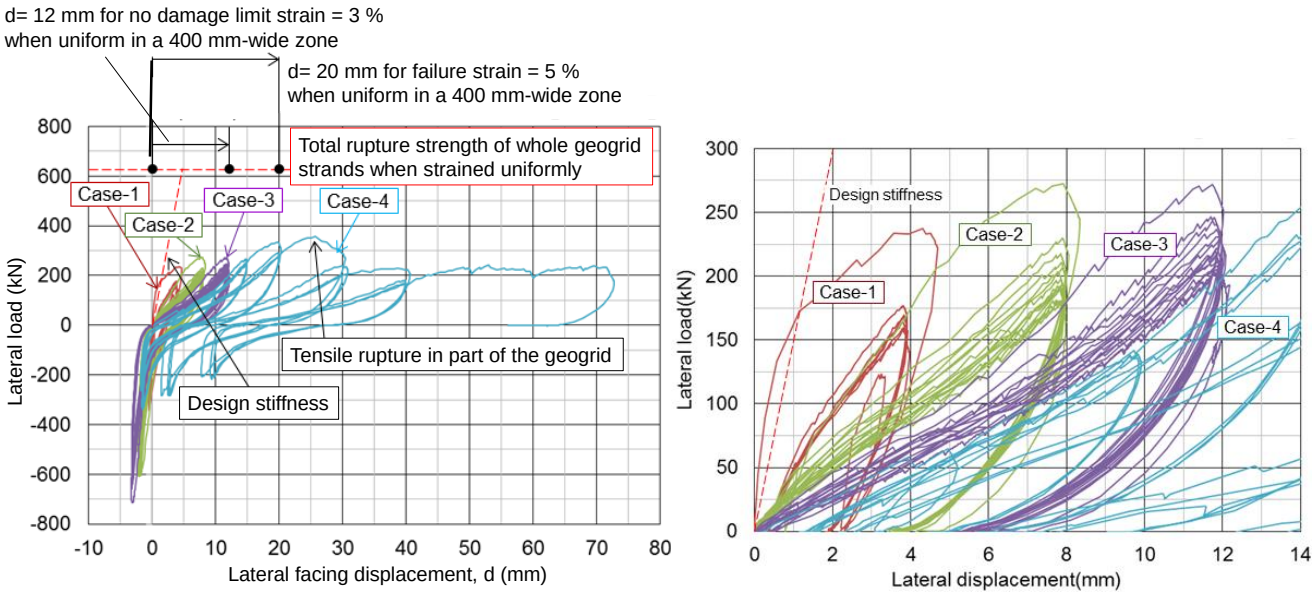

Figure 6. Relationships between lateral load and displacement of FHR facing, Cases 1, 2, 3 and 4: (a) whole relations; and (b) enlarged relations in the active state.

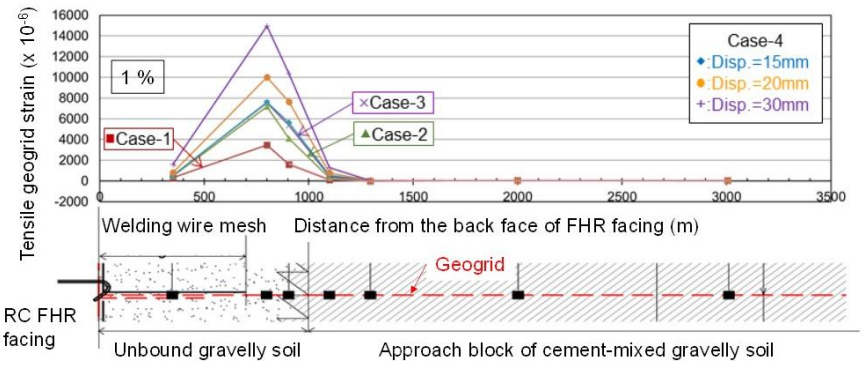

Figure 7. Distributions of geogrid strains measured with electric-resistance gauges in Cases 1, 2, 3 & 4.

Fig. 7 shows the distributions of tensile strain in the geogrid layer measured at the end of loading in each of Cases 1, 2 and 3 and at different displacements in Case 4. Although the measurement is not dense enough to capture the details, it may be seen that the strain is concentrated in the free zone between the welding wire mesh and the approach block of cement-mixed gravelly soil. In the zone where a welding wire mesh and a geogrid layer are overlapping, the development of geogrid tensile stain is largely restrained by the friction along the interface with a welding wire mesh framework (having a stiffness larger by a factor of more than 50 than the geogrid layer) and the other with unbound gravelly soil. The geogrid strain at 1.3 m from the back of the FHR facing, inside the approach block, is nearly zero. That is, most of the tensile deformation of the geogrid takes place in a 30 cm-wide free zone with only part in a narrow (about 10 cm-wide) tail end zone of the welding wire mesh and a very narrow front zone of the approach block. The largest lateral displacement in Case 3, where the geogrid is not noticeably damaged, is equal to 12 mm, for which the average geogrid strain is 3 % in a 40 cm-wide zone including a 30 cm-wide free zone. When the displacement at the maximum tensile resistance is conservatively defined to be equal to 20 mm in Case 4 (Fig. 6a), the average geogrid strain at tensile rupture in the 40 cm-wide zone is 5 %.

The stiffness when subjected to passive compressive loads is much higher and stable when compared with the one when subjected to active tensile loads.

Before this study was performed, the relation of a broken line starting from the origin shown in Fig. 6 was used as the lateral load-displacement relation of the buffer zone under long-term ordinary and seismic conditions in the design of GRS integrated bridge shorter than 20 m in span. It may be seen that this relation is representative of the initial relation in Case 1. Subsequently, in the design against thermal deformation and concrete drying shrinkage of the girder and seismic loading of GRS integral bridges longer than 20 m, including the one with a span of 60 m (Fig. 9), a slope that is a half of the value of the broken line was used by taking into account likely stable degradation by thermal cyclic loading. This trend can be confirmed by the behavior in Cases 2 and 3 simulating thermal cyclic deformation (Fig. 6). In fact, the geogrid was not seriously damaged by the end of Case 3, where the maximum lateral displacement was 12 mm with an average geogrid strain of 3 %. In Case 4 (simulating very severe seismic loading), the geogrid layers started rupturing progressively as the lateral displacement exceeded 20 mm (i.e., an average geogrid strain of 5 %). Yet, a nearly constant residual peak tensile load was maintained, which was approximately a half of the maximum peak load. In the current seismic design code, this trend is taken into account in such that a bi-linear relation with an initial stiffness equal to 1/8 – 1/3 (smaller for larger thermal deformation) of the value of the broken line while upper-bounded by the peak load lower than a half of the peak value observed in Case 4 is specified.

The model was excavated after the cyclic loading tests. The geogrid exhibited tensile rupture in the free zoon (Figs. 8a & b), while the connection between the FHR facing and the buffer zone was undamaged (Figs. 8c & d), indicating that the anchor steel rods arranged to ensure a high connection strength functioned effectively. These results were referred to in the design of GRS integral bridges.

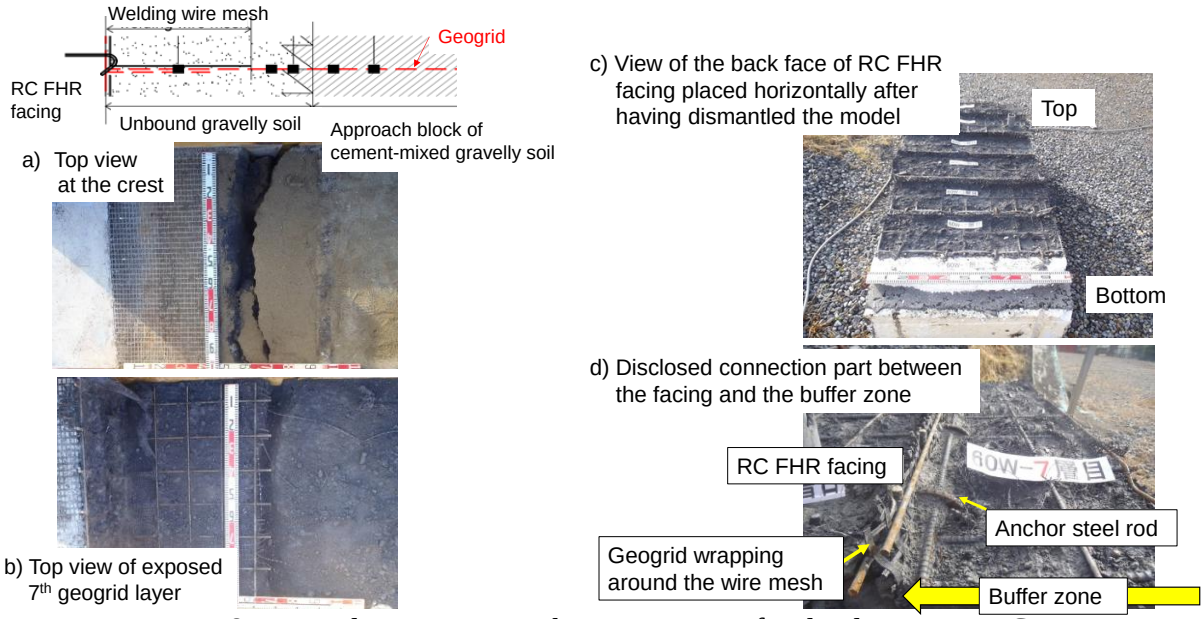

Figure 8. Internal structure seen by excavation after loading tests in Case 4.

3 FIELD MEASURING OF GRS INTEGRAL BRIDGE WITH SRC-THROUGH GIRDER

Among three GRS integral bridges for Sanriku Railway constructed in place of the simple girder bridges that totally collapsed by a great tsunami of the 2011 Great East Japan Earthquake, Haipe-sawa Bridge has the longest span, 60 m (Fig. 9; Tatsuoka et al., 2016; Soga et al., 2018). The width of the girder for a single track is 6.7 m. Both ends of a continuous girder is structurally integrated to the top of the FHR facings of a pair of GRS RWs while supported by a central pier designed to resist only vertical loads. A through girder was employed to ensure a sufficient free height below the girder for a local road under-passing the bridge. In addition, prepared for relatively large thermal length changes of this relatively long SRC girder, the width of the buffer zone was made 1.0 m as the full-scale model tests (Fig. 5a), compared with a width of 40 cm comprising gravel-filled bags employed with the full-scale model (Fig. 2) and other shorter prototypes. Welding wire mesh frameworks as used in the full-scale model (Figs. 5a & c) were used in place of geogrid bags. To confirm the relevance of the design and construction of the bridge, the behaviour from during construction and for a period of 2.5 years after completion was carefully monitored.

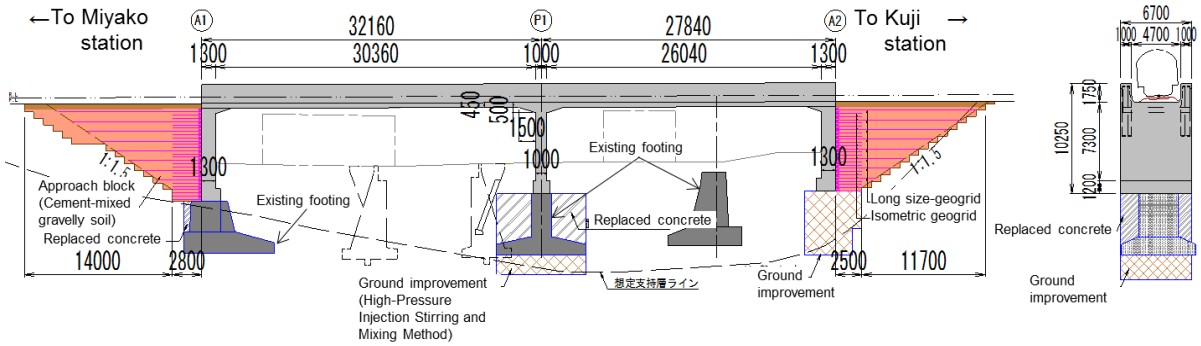

Figure 9. Haipe-sawa Bridge, Sanriku Railway (all units in mm) (Tatsuoka et al., 2016).

Fig. 10a shows the time histories of ambient temperature, temperature inside the girder and lateral displacements at the top and bottom of the FHR facing relative to the approach block at both sides of the bridge. The girder expands and shrinks as the temperature rises and drops, while the lateral displacements of the FHR facings on both sides are nearly the same. The amplitude at the top of the facing at each side is equal to about 6 mm, whereas it is less than 1 mm at the bottom of the facings. This observed amplitude equal to about 6 mm by a temperature amplitude of about 30°C (i.e., 0.2 mm/°C) is much smaller than the largest value equal to 15 mm/50°C (i.e., 0.3 mm/°C) for a 60 m-long RC girder simulated in Case 3 in the full-scale model test (Table 1). That is, the test conditions in the full-scale model test cover the field conditions of this bridge. Fig. 10b shows the relationship between the temperature inside the girder and the total deformation of the girder, which is defined zero when the girder was completed and integrated to the top of the FHR facings in 1 November 2013 (i.e., the start of the plot in Fig. 10a). In Fig. 10b, the deformation at 6:00 AM in each day was plotted to exclude daily fluctuations. A broken line indicates the relation when the girder deforms freely by ambient temperature changes (i.e., the free relation). This was obtained by assuming that the average thermal expansion coefficient of the girder is the same as the value of steel, equal to 12μ/℃, as the structure of the girder is SRC having a large volume of steel while the bottom flange is exposed to the atmosphere.

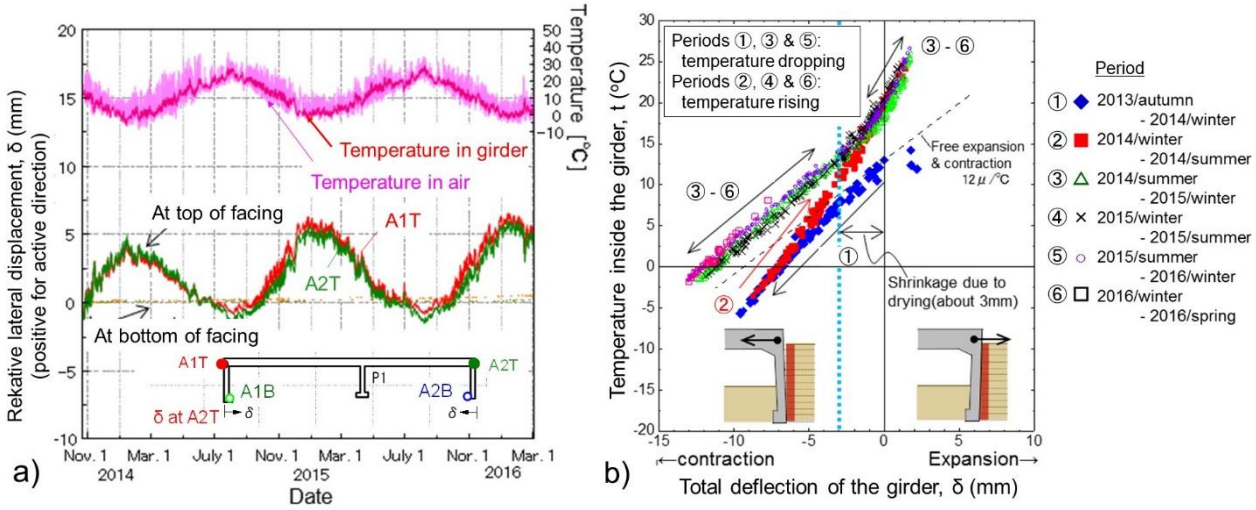

Figure 10. a) Post-construction time histories of temperature and displacements at the top and bottom of the FHR facings relative to the approach blocks: and b) their relationship. Haipesawa Bridge, Sanriku Railway.

The following trends may be seen from Fig. 10b. In term 1 starting upon the completion of the bridge, the girder contracted by a temperature drop and drying shrinkage of concrete, which decreased the active earth pressure. The fact that the slope of the measured relation is slightly larger than the free relation may indicate that the friction at the interface between the geogrid and the welding wire mesh and the one between the geogrid and the gravelly soil were initially fully mobilized and the geogrid layers exhibited some initial resistance against the girder contraction. In term 2, the girder expanded by a temperature rise. The slope of the relation is larger than term 1, showing some effective passive resistance associated with the lateral compression of the approach fill. In term 3 and subsequent terms, the relation is nearly fully reversible and stable without exhibiting an increase in the residual girder deformation, which would take place if the earth pressure increases continuously by the ratcheting phenomenon during cyclic loading

(Tatsuoka et al., 2009, 2010). When the girder deformation becomes positive in expansion (i.e., when the girder becomes longer than the initial value when the girder was integrated to the FHR facings), the slope of the relation becomes much steeper than the free relation. On the other hand, when the girder deformation becomes negative (i.e., when the girder becomes shorter than the initial value), the slope becomes nearly the same as the free relation. More precisely, the slope changes at a girder deformation equal to about - 3 mm. It seems that the unbound gravelly soil in the free zone in the buffer zone exhibited active yielding filling a small space created by this girder shrinkage one time in term 3 while no such yielding was repeated during the subsequent periods. These trends are consistent in a broad sense with the behaviour observed in the full-scale model test (Fig. 6a) in that the FHR facing exhibits much larger resistance against push-in load by girder expansion than against pull-out load by girder contraction. Besides, the slope when the girder is shorter than the initial value in terms 3 – 6 is nearly the same as the free relation while noticeably smaller than the one in term 1. This trend is due likely to that the stiffness of the geogrid in the buffer zone had decreased by cyclic loading, as observed in the full-scale model tests (Fig. 6). Finally, the largest contraction in terms 3 - 6 is larger by about 3 mm than the largest value in term 1. This indicates that the concrete of the girder exhibited most drying shrinkage in the first year (i.e., in terms 1 and 2). This value, 3 mm, is nearly the same as the value theoretically obtained by assuming that the whole of the 60 m-long girder exhibits a uniform drying shrinkage strain of 50 μ.

4 CONCLUSIONS

The buffer zone between the FHR facing and the approach blocks of cement-mixed gravelly soil in the abutment of GRS integral bridge comprises unbound gravelly soil, geogrid layers and welding wire mesh. Its load-deformation properties control the residual forces in the bridge system caused mainly by annual thermal deformation, concrete drying shrinkage of the girder and seismic loading. Lateral cyclic loading tests was performed on a full-scale partial model of the abutment including a buffer zone simulating these loading conditions. This factor becomes more important as the bridge span becomes longer, in particular longer than 20 m. The post-construction behaviour of a 60 m-long prototype GRS integral bridge validated the design and construction method developed based on the results of the model tests. Several other GRS integral bridges have been constructed, or are at the stage of design, following this design method (Tatsuoka et al., 2016; Soga et al., 2018).

REFERENCES

Nagatani, T., Tamura, Y., Iijima, M., Tateyama, M., Kojima, K. and Watanabe, K. 2009. "Construction and field observation of the full-scale test integral bridge", Geosynthetics Engineering Journal, Vol.24, pp.219-226.

Soga, D., Takano, Y., Yonezawa, T., Koda, H., Tateyama, M. and Tatsuoka, F. 2018. Design and construction of various type GRS structures for a new high-speed railway, *Proc. 11ICG*, Seoul.

Tatsuoka, F. 1992. "Roles of facing rigidity in soil reinforcing", Keynote Lecture, *Proc. Earth Reinforcement Practice, IS-Kyushu '92 (Ochiai et al. eds.)*, Vol.2, pp.831-870.

Tatsuoka, F., Tateyama, M, Uchimura, T. and Koseki, J. 1997. "Geosynthetic-reinforced soil retaining walls as important permanent structures", Mercer Lecture, *Geosynthetic International*, Vol.4 (2), pp.81-136.

Tatsuoka, F., Hirakawa, D., Nojiri, M., Aizawa, H., Nishikiori, H., Soma, R., Tateyama, M. and Watanabe, K. 2009. A new type integral bridge comprising geosynthetic-reinforced soil walls, *Gesynthtetics International*, IS Kyushu 2007 Special Issue, Vol.16, No.4, pp.301-326.

Tatsuoka, F., Hirakawa, D., Nojiri, M., Aizawa, H., Nishikiori, H., Soma, R., Tateyama, M. and Watanabe, K. 2010. "Closure to Discussion on A new type of integral bridge comprising geosynthetic-reinforced soil walls", *Gesynthtetics International*, Vol.17 (4), pp.1-12.

Tatsuoka, F., Tateyama, M., Koda, M., Kojima, K., Yonezawa, T., Shindo, Y. and Tamai, S. 2016. Research and construction of geosynthetic-reinforced soil integral bridges, *Transportation Geotechnics*, Vol.8, pp.4-25.

Tatsuoka, F., Soma. R., Nishikiori, H., Watanabe, K. and Hirakawa, D. 2018, Higher seismic performance of GRS integral bridge by cement-mixing the approach fill, *Proc. 11ICG*, Seoul.

Koda, M., Nonaka T., Suga M., Kuriyama R., Tateyama M., and Tatsuoka, F. 2013. "Lateral cyclic loading tests of a full-scale GRS integral bridge model", *Proc. International Symposium on Design and Practice of Geosynthetic-Reinforced Soil Structures*, Bologna, pp.157-174.